An original methodology to study polymeric nanoparticle-macrophage interactions: Nanoparticle tracking analysis in cell culture media and quantification of the internalized objects

Tom Bourguignon, Adriano Torrano, Ludivine Houel-Renault, Arnaud Machelart, Priscille Brodin, Ruxandra Gref

Title:

An original methodology to study polymeric nanoparticle-macrophage interactions: nanoparticle tracking analysis in cell culture media and quantification of the internalized objects

Authors

Tom Bourguignon[1], Adriano A. Torrano[2], Ludivine Houel-Renault[1], Arnaud Machelart[3], Priscille Brodin[3] and Ruxandra Gref[1]*

[1]Université Paris-Saclay, CNRS, Institut des Sciences Moléculaires d'Orsay, 91405, Orsay, France

[2]University of Munich (LMU), Department of Chemistry and Center for NanoScience (CeNS), 81377 Munich, Germany

[3]Université de Lille, CNRS, INSERM, CHU Lille, Institut Pasteur de Lille, U1019 - UMR 9017 - CIIL - Center for Infection and Immunity of Lille, F-59000 Lille, France

*Corresponding author:

Dr. Ruxandra Gref

Université Paris-Saclay, CNRS, Institut des Sciences Moléculaires d'Orsay, 91405, Orsay, France. Tel: +33 (1) 69158234; E-mail: ruxandra.gref@universite-paris-saclay.fr.

Abstract

Poly(lactic acid) (PLA) and poly(lactic-*co*-glycolic acid) (PLGA) are among the most employed (co)polymers for the preparation of drug nanocarriers for the treatment of cancer and infectious diseases. Before considering any clinical use, it is necessary to understand the interactions between polymeric nanoparticles (NPs) and their physiological environment, especially immune cells. Here, we propose a simple, yet precise method to assess NPs internalization kinetics in macrophages, based on the direct analysis of the cell culture media after different incubation times. The proof of concept is given here by using fluorescent PLGA NPs. Nanoparticle tracking analysis (NTA) was a method of choice, enabling detecting each individual NP and analyzing its trajectory while in Brownian motion. As compared to dynamic light scattering (DLS), NTA enabled a more precise determination of NP size distribution. The uptake process was rapid: in one hour, around a third of the NPs were internalized. In addition, the internalized NPs were visualized by confocal microscopy. The fluorescent cellular stacks were analyzed using a freely available macro for ImageJ software, Particle_In_Cell-3D. The internalized objects were localized and counted. This methodology could serve for further studies while analyzing the effects of NPs size, shape and surface properties on their interaction with various cell lines.

Keywords: polymer nanoparticle; poly(lactic acid); size distribution; cellular uptake; nanoparticle tracking analysis; dynamic light scattering; confocal microscopy

1. Introduction

Drug nanocarriers are able to efficiently incorporate, protect towards degradation and ferry active molecules from the administration site to diseased organs, tissues and cells. They are gaining increasing interest for the treatment of severe diseases such as cancer and multiresistant infections (Zhao et al., 2019). While liposomes, discovered early in the 1960s, were the first nanotechnology-based drug delivery system (Finean and Rumsby, 1963), a plethora of other nanocarriers have been developed, including polymeric, hybrid organic-inorganic or metal nanoparticles (NPs), micelles, nanogels, dendrimers, carbon nanotubes and quantum dots. Recently, several nanotechnologies such as Onpattro and Vyxeos were approved by the Food and Drug Administration (FDA), and nowadays, the NP-based vaccines represent a cornerstone in the fight against the COVID-19 pandemic (Jones et al., 2019; Sharma et al., 2021).

In particular, polymeric materials have been studied and engineered for more than fifty years, with applications ranging from resorbable sutures and orthopedic implants to nano(micro)particles. The biocompatible and biodegradable poly(lactic acid) (PLA) and poly(lactic-*co*-glycolic acid) (PLGA) are nowadays among the most employed synthetic polymers used to produce drug nanocarriers (Zielińska et al., 2020). A plethora of drug-loaded NPs were produced by various methods aiming to control the main parameters which govern the NPs' *in vivo* fate: size distribution, shape, surface charge and composition. Thus, NPs with increased blood circulation times and targeting abilities were prepared, depending on the application they were destined to (Gref et al., 1994; Ulbrich et al., 2016). The main preparation methods of PLA/PLGA NPs are nanoprecipitation and emulsification-solvent evaporation.

Developed in 1989 by Pr. Fessi and his team (Miladi et al., 2016), nanoprecipitation is regarded as a quite simple and reproducible technique that allows the obtaining of submicron-sized

polymeric particles. It consists in adding in a drop-by-drop fashion, in an aqueous solution, a polymer in a water-miscible solvent. This results in the immediate precipitation of the polymer under the form of NPs, based on solvent displacement. In emulsification-solvent evaporation, the polymer is dissolved in a volatile solvent non-miscible with water, and an emulsion is formed with an aqueous solution. The droplet size is generally reduced by sonication and the solvent is finally removed. By adjusting the preparation parameters, both NP preparation processes have the potential to be tuned to yield NPs with specific characteristics while maintaining reproducible results (Legrand et al., 2007; Hernández-Giottonini et al., 2020).

Upon intravenous administration, NPs interact with cells of the immune system (such as macrophages) which readily recognize them as foreign and withdraw them from blood circulation. NP-macrophage interactions depend on the size and shape of the NPs (Nicolete et al., 2011; Hoshyar et al., 2016; Rattan et al., 2017; Boltnarova et al., 2021). In view of developing medical applications, the fast-growing field of nanomedicine is in need for reliable and convenient methodologies to precisely assess the NPs' size distribution and to investigate their interaction with cells.

Nowadays, several techniques are available to determine the NPs' size distribution. The most widespread ones are: i) dynamic light scattering (DLS), the most common and user-friendly method, which allows to estimate the mean NPs' hydrodynamic diameter and polydispersity, but can lead to size overestimations and difficulties in discriminating sub-populations of polydisperse NPs samples (Filipe et al., 2010), and ii) transmission electron microscopy (TEM) and atomic force microscopy (AFM), which allow for an excellent resolution and a precise evaluation of the NPs' diameters, but require a sometimes complex and time-consuming sample preparation, as well as the investigation of large enough NPs populations to enable statistically relevant results (Hoo et al., 2008; Chicea, 2012). In the case of PLA/PLGA NPs, cell internalization processes

are generally studied by confocal microscopy, with the aim of comparing NPs formulations, and without quantitative analysis. For quantitative investigations of the internalized amounts, labeled NPs (mostly radioactive ones) are used (Gref et al., 2003; Wu et al., 2020).

In this context, we propose here a straightforward method to both accurately characterize NPs size distribution and quantify their interaction with cells. Nanoparticle tracking analysis (NTA) was employed as a means to characterize NPs and investigate their stability in complex media mimicking physiological conditions, as well as to track and quantify their internalization inside immune cells. This method relies on dynamic light scattering to analyze individual NPs' trajectories in their Brownian motion. Advantageously, NTA also allows determining NPs concentration within the sample and possible aggregation events. So far, NTA was only used for the sole purpose of characterizing NPs, like DLS. NTA was sometimes employed to monitor the excretion of exosomes collected from cell cultures (Soo et al., 2012; Zheng et al., 2012), but never yet to study NP-cell interactions.

The novelty here is that NTA is used to assess the polymeric NPs internalization kinetics, which has, to our knowledge, never been described before. The proposed method is simple and reproducible. It consists in incubating the NPs with macrophages for different times, harvesting the cell culture media and directly analyzing it by NTA, after appropriate dilution. Thus, the concentration of the NPs in contact with the cells could be accurately determined at each time point. By difference, it was possible to determine the fraction of cell-interacting NPs. To allow the study, the PLGA NPs were labelled with rhodamine (Rho) covalently grafted onto the polymer chain ends, to avoid any leakage during the experiments. Furthermore, to complement these studies, confocal experiments were carried on allowing visualizing NPs and NP aggregates within the cells or at their surface. Particle_In_Cell-3D, an ImageJ macro specially designed for this purpose, was used to count the number of fluorescent objects inside the macrophages

(Torrano et al., 2013). Advantageously, this approach allowed to highlight large differences in NPs internalization between cells in the same well. In short, we propose a precise and user-friendly method to not only characterize NPs after interaction with cells, but also to quantify their internalization kinetics.

2. Experimental

2.1. Materials and reagents

The biodegradable PLGA (50/50) copolymer was a kind gift from Expansorb (Aramon, France). PLA ester-terminated (molecular weight (MW) = 10-18 kDa), PLA acid-terminated (MW = 18-24 kDa), rhodamine B (Rho), polyvinyl alcohol (PVA) (88% hydrolyzed), piperazine, trimethyl aluminum ($AlMe_3$), 4-dimethylaminopyridine (DMAP), 1-ethyl-3-(3-dimethylaminopropyl) carbodiimide (EDC), calcium chloride (NaCl), potassium chloride (KCl), calcium chloride ($CaCl_2$), magnesium chloride ($MgCl_2$), potassium hydroxide (KOH), dichloromethane (DCM) and RBS 35 concentrate were purchased from Sigma-Aldrich (Saint-Quentin-Fallavier, France). Dulbecco's phosphate buffered saline (DPBS), Dulbecco's modified Eagle medium (DMEM), fetal bovine serum (FBS) and penicillin/streptomycin were purchased from Gibco (Illkirch, France). Ethanol 96% and acetone 100% were purchased from VWR Chemicals (Fontenay-sous-Bois, France). HEPES was purchased from Acros Organics (Illkirch, France). Paraformaldehyde (PFA) 16% was purchased from Electron Microscopy Sciences (Nanterre, France). CellMask Deep Red was purchased from Invitrogen (Illkirch, France). Pure water used in all experiments was filtered (18.4 M cm) by a Milli-Q system (Millipore, Milford, MA, USA).

2.2. Synthesis of PLA-Rho

PLA grafted with Rho at the terminal carboxyl chain end (PLA-Rho) was synthesized by adapting a previously described method (Nguyen and Francis, 2003; Pancani et al., 2018). Briefly, 11.3 mL of a 2 M solution of $AlMe_3$ in toluene were added to 17.5 mL of a 0.22 mg/mL solution of piperazine in DCM. The reaction mixture was refluxed for 24 h at 50°C with Rho (0.5 mg/mL) under inert atmosphere. The obtained Rho-piperazine amide was extracted, purified and dried. 5 mg of Rho-piperazine amide were then reacted with 50 mg of PLA acid-terminated, using DMAP as catalyst and EDC as coupling agent. The obtained Rho-PLA was extracted, purified and dried.

2.3. Preparation of NPs by emulsification-solvent evaporation

An aqueous solution of PVA (0.5% w/v) was prepared by dissolving 150 mg of PVA in 30 mL of Milli-Q water. In order to prepare an aqueous suspension of NPs (15 mg/mL), 60 mg of PLGA were solubilized in 1.5 mL of DCM in a glass vial under magnetic stirring. Then, 4 mL of the PVA solution were added in the vial, followed by vortexing for 20 s to form a coarse emulsion. A fine emulsion was obtained by sonication for 90 s (20% of power), using a sonicator probe (Sonopuls HD 2070, BANDELIN Electronic GmbH & Co, Berlin, Germany). The size of the oil droplets was further reduced by a second sonication step, in an ice bath (30 s, 10% of power). The solvent (DCM) was evaporated overnight under gentle magnetic stirring. Fluorescent NPs were prepared by the same method, by adding 0.2 mg PLA-Rho in the PLGA DCM solution.

2.4. Preparation of NPs by nanoprecipitation

To prepare NPs by nanoprecipitation, 75 mg of PLGA were first solubilized in 1 mL of acetone in a glass vial. Then were added 0.2 mg of PLA-Rho from a stock solution of PLA-Rho, and the resulting solution was diluted with acetone to a final polymer concentration of 12.5 mg/mL.

After, 100 µL of this polymer solution were added drop by drop in 1 mL of PVA aqueous solution (0.5% w/v) under magnetic stirring (650 rpm). NPs formed immediately and the suspension was maintained under stirring until complete evaporation of acetone.

2.5. NPs characterization

Three different techniques were used to determine the morphology and the size distribution of the NPs. First, TEM investigations were performed using a JEOL JEM-1400 microscope operating at 80 kV. To do so, 4 µL of NP suspensions (concentration ranging between 1 and 15 mg/mL) were deposited onto copper grids covered with a formvar film (400 mesh) for 60 s. The samples were then stained using 2% phosphotungstic acid for 30 s. The excess liquid was blotted off using filter paper, and the grids were dried before observation. Images were acquired using a post-column high-resolution (9 megapixels) high-speed camera (RIO9, Gatan) and processed with ImageJ.

The NPs' mean hydrodynamic diameter was also determined by DLS using a Malvern Zetasizer (Nano ZS90, Malvern Panalytical, Worcestershire, UK), with an equilibration time of 120 s. The analyzed samples were diluted using Milli-Q water, aiming for a concentration range of 10 to 100 µg/mL, and the mean diameters were reported as $Z_{Average}$ (nm) ± standard error (SE), with a PdI lower than 0.2. All experiments were performed in triplicate.

The NPs' average hydrodynamic diameter and concentration were also evaluated by NTA (NanoSight LM10, Malvern Panalytical, Worcestershire, UK). 1 mL of the sample was introduced in the device's chamber, with a concentration range of 1 to 5 µg/mL, which corresponds to an approximate concentration of 10^8 objects/mL. Once the NPs were exposed to a laser beam, the light scattering and Brownian motion were both recorded on video and analyzed, which allowed to characterize the NPs individually. For each sample, five videos of 60 s each

were recorded. In order to be certain that only NPs would be visualized and analyzed, a fluorescence filter was applied all through the recordings.

2.6. NPs intracellular internalization using NTA and confocal microscopy

The J774A.1 cell line was obtained from ATCC and cultured at 2×10^5 cells/mL, using DMEM medium supplemented with 10% FBS and 1% penicillin/streptomycin at 37°C and 5% CO_2. When studying NPs internalization, 5×10^5 cells in 1 mL of medium were deposited on cover glasses at the bottom of 6-well plates. Cover glasses had been previously sterilized by immersion in an aqueous solution of RBS (2%) at 50°C before being dipped in 90% ethanol and dried under a biological hood before use. Then, cells were incubated at 37°C and 5% CO_2 overnight. The next day, the medium was removed and replaced with 1 mL of medium containing 4×10^{10} NPs. After different incubation times (from 1 to 24 h), supernatants were harvested and diluted in Milli-Q water before being analyzed by NTA.

HEPES buffer (20 mM HEPES, 140 mM NaCl, 2.5 mM KCl, 1 mM $CaCl_2$, 1 mM $MgCl_2$, pH adjusted to 7.4 with KOH) was prepared for the analysis of cells on cover glasses, in order to ensure pH homeostasis and avoid osmotic pressure changes. Cover glasses were placed in 300 µL of CellMask Deep Red (1 X, diluted in HEPES buffer), a cell membrane marker, for 5 min at 37°C. A fixation solution comprising HEPES buffer and PFA (3.75%) was prepared. The membrane marker was removed and cover glasses were placed in 1 mL of the fixation solution for 5 min at 37°C. The fixation solution was then removed and cover glasses were cleaned three times in DPBS.

Confocal microscopy was performed immediately with a Leica TCS SP5 device (AOBS, Mannheim, Germany) equipped with a Leica objective (63×/1.4 NA, oil immersion). For Rho

imaging was used the 514 nm line of a continuous Ar laser, and for CellMask Deep Red imaging, the 633 nm line of a continuous He-Ne laser. Images were produced in direct slow scanning sequential mode (400 Hz) and the fluorescence was collected in the spectral range from 520 to 600 nm for Rho, and from 640 to 680 nm for CellMask Deep Red. The resolution of the confocal images was 512×512 pixels, recorded on 8 bits with different zoom values and a pinhole size of 1 airy. Their size in µm depended on the zoom (between 2 and 4). Images stacks were acquired in order to observe all the layers of the cells with a step of 0.130 µm (around a hundred images were necessary). The stacks were then analyzed using ImageJ, with a macro (Torrano et al., 2013) aiming to create cell masks, 3D representations of cells from the stacks, and to quantify intracellular NPs.

3. Results and discussions

3.1 DLS and NTA: characteristics and assets

Three simultaneous goals were pursued here: i) accurately determine the size distribution of the polymeric NPs; ii) study their stability in biological medium, and iii) quantify their internalization kinetics inside macrophages. The NPs' size distribution is commonly determined by DLS, a well-known and non-destructive method schematized in **Fig. 1. A**. Briefly, the principle of this method consists in illuminating a suspension of NPs with a laser source. The intensity of the light scattered by the NPs in their Brownian motion is measured at a given angle (typically 90°) allowing to estimate the mean hydrodynamic diameter and size distribution of the sample. Through its simplicity of use, DLS is a widespread method; however, it only allows to study populations of NPs, with no possibility of observing individual objects. Thus, in the case of a relatively polydisperse NP population, DLS is not well adapted to discriminate sub-populations.

Moreover, the largest NPs scatter more light than the smaller ones, leading to an overestimation of the mean hydrodynamic diameters (Filipe et al., 2010; Varenne et al., 2016).

Addressing the challenge of estimating accurately the size distribution of a polydisperse NP sample thus requires a method which would allow to study populations of NPs and individual objects at the same time (Chaupard et al., 2021). Microscopies such as TEM and AFM enable to determine the size of isolated NPs with a high resolution, but besides requiring an experimented user and a sometimes complex sample preparation, it is cumbersome to analyze populations large enough to obtain representative results.

In this context, NTA is an interesting alternative. The NPs in the device's chamber are illuminated by a laser beam, which makes them appear as bright spots. This enables to visualize and track the trajectories of individual NPs in their Brownian motion using a classic optical microscope. (**Fig. 1. B**). From the trajectories of thousands of NPs, individual hydrodynamic diameters are calculated using the Stokes-Einstein equation. Contrary to DLS, which analyzes "bulk" samples, NTA allows to reconstitute size distributions from individual NPs measurements. Another advantage is that, considering the analyzed volume is known, NTA allows to calculate the concentration of the sample. Finally, the device can be equipped with fluorescence filters, which allow to track only the fluorescent objects in the sample. This is an asset in studying NPs in complex environments such as serum-containing cell culture media. A recording without (**Supplementary material 1**) or with a fluorescence filter on (**Supplementary material 2**) is available in the supplementary materials.

[Figure 1]

NTA and DLS were comparatively used here to determine the NPs' size and to investigate their interactions with macrophages. First, fluorescent PLGA NPs were successfully prepared by two methods, nanoprecipitation and emulsification-solvent evaporation. They were named NPs-P and NPs-E, respectively. The fluorescent dye Rho was covalently grafted onto the polymeric cores, to avoid any leakage during the experiments (Pancani et al., 2018). Both types of NPs appeared round-shaped and with homogeneous sizes when observed by TEM (**Fig. 2**). The images also showed a more polydisperse population of NPs-E (**Fig. 2. B**) than NPs-P (**Fig. 2. A**). After analyzing a hundred objects, the mean diameters were 78 ± 28 nm and 117 ± 50 nm for NPs-P and NPs-E respectively.

The suitability of NTA for studying these fluorescent NPs was further investigated. Indeed, knowing that the NPs would be investigated in complex media such as cell culture media, it was important that they would be visible with a fluorescence filter on, so that only them would be detected, and no other parasite object from the medium. Thus, both samples, NPs-P and NPs-E, were analyzed with and without a fluorescence filter.

Without the fluorescence filter, NPs-P exhibited a concentration of $4.45\times10^{8} \pm 2.07\times10^{7}$ particles/mL, and a mean hydrodynamic diameter of 171 ± 36 nm. With the fluorescence filter, the concentration was $3.24\times10^{8} \pm 1.54\times10^{7}$ particles/mL, and the mean hydrodynamic diameter, 159 ± 39 nm (**Fig. 2. C**). For NPs-E, without the fluorescent filter, the concentration was $5.53\times10^{8} \pm 1.38\times10^{7}$ particles/mL, and the mean hydrodynamic diameter, 260 ± 80 nm. With the fluorescence filter, the values were $4.03\times10^{8} \pm 1.16\times10^{7}$ particles/mL for the concentration, and 280 ± 94 nm for the mean hydrodynamic diameter (**Fig. 2. D**).

One result to notice is that the size distribution confirms what could be seen on the TEM images: for NPs-P, a very narrow size distribution can be observed, which supports the idea of a monodisperse population. For NPs-E, however, several peaks were recorded, indicating the presence of a quite polydisperse population. Another observation is that with the fluorescent filter on, ~ 27% of the NPs-P and the NPs-E were not detected by the device. Such an observation can be explained by the fact that with the filter on, the image perceived by the camera is generally darker, and thus, focusing on the NPs is more difficult. In this context, in order to optimize the investigations, a higher quantity of Rho could be incorporated into the NPs. However, this partial detection does not seem to have any influence on the mean hydrodynamic diameter evaluation. In short, some objects might go unnoticed, but both NPs-P and NPs-E are efficiently detected and analyzed with the fluorescence filter on.

Finally, the question of whether cell culture medium would interfere with NPs detection or not was of utmost importance. NPs-P and NPs-E were suspended in cell culture medium at a suitable concentration for NTA and analyzed with and without the fluorescence filter. With the filter, NPs-P exhibited a concentration of $4.01\times10^{8} \pm 9.95\times10^{6}$ particles/mL and a mean hydrodynamic diameter of 150 ± 39 nm (**Fig. 2. E**), while NPs-E showed a concentration of $1.83\times10^{8} \pm 5.48\times10^{6}$ particles/mL and a mean hydrodynamic diameter of 250 ± 101 nm (**Fig. 2. F**). For both samples, the size distribution remained the same as in Milli-Q water (indicating that the NPs did not aggregate) (**Fig. 2. C** and **D**). As a conclusion, fluorescent NPs can be analyzed efficiently by NTA in complex media, provided the adequate fluorescence filter is on. Indeed, without the filter, so many objects were detected that the software could not complete the analysis.

[Figure 2]

3.2 Comparison of NTA and DLS results

It is established in the literature that DLS can sometimes overestimate the mean hydrodynamic diameter, if the sample contains aggregates or bigger sub-populations (Filipe et al., 2010). This observation was put to the test with the studied NPs-P and NPs-E samples. On **Fig. 3. A** and **B**, screenshots taken during the NTA analysis of NPs-P and NPs-E, respectively, can be seen. The recorded trajectories of the NPs can also be observed. On **Fig. 3. C** and **D**, the results of both NTA and DLS analyses are displayed.

A first observation is that for both NPs-P and NPs-E, the mean hydrodynamic diameters calculated by DLS are larger than the ones determined by NTA. Differences as high as 50 nm were observed in the case of NPs-E. The second finding concerns the size distribution recorded by DLS. For NPs-P, the DLS size distribution is narrow, similarly to the NTA one. But for NPs-E, the DLS distribution is much broader and, more importantly, does not reflect the several populations which were detected by NTA (**Fig. 2. D**). These findings show that, despite the fact that DLS is a rapid and user-friendly method, it might overestimate the mean hydrodynamic diameter and, furthermore, not be able to discriminate sub-populations in a polydisperse sample. Finally, NTA appears to be an adequate alternative to TEM and DLS, being able to analyze important NP populations on an individual basis and within a short timeframe.

[Figure 3]

3.3 Study of NP internalization kinetics by NTA

This study proposes a use of NTA which, to our knowledge, has never been described in the literature before. The objective was to quantify the internalization of NPs by macrophages in a

simple and reproducible manner. For the proof of concept, NPs-E were put to incubate with J774A.1 macrophages for different time periods, from 1 to 24 h. The cell culture media containing the NPs not engulfed or not adhered to the macrophages were recovered. After a suitable dilution with Milli-Q water, NTA experiments were performed with the NP suspensions. The postulate was that all NPs which were not present in the cell culture media had interacted with the macrophages. Therefore, by knowing the initial concentration of NPs incubated with the macrophages at the start of the experiment and by measuring the NP concentration in the collected cell culture media, it was possible to track the NPs' internalization kinetics.

Fig. 4 shows the results obtained by incubation of NPs-E suspensions at an initial concentration of 200 µg/mL with macrophages, and the control experiment, corresponding to the NPs incubation at 37°C in cell culture medium, in the same conditions, but without macrophages. The concentration of NPs-E which were incubated for 24 h in the absence of cells would remain the same. The mean hydrodynamic diameter was of 292 ± 11 nm, similarly to what was observed in Milli-Q water, suggesting that no aggregation occurred (**Fig. 2. D**). In contrast, when the same NPs were incubated with macrophages, the NPs concentration was dramatically reduced, indicating that interactions took place with the macrophages.

The internalization process occurred in two phases: a first one, rapid (1 h), during which around a third of the NPs were internalized; and a second one, until the end of the study, during which NPs were internalized in a slower manner. One hypothesis is that the macrophages which were present from the beginning of the experiment internalized a large amount of NPs until reaching saturation, and that cell growth progressively produced new macrophages which continued internalizing the NPs remaining in the supernatants. Another possibility is that NPs progressively sediment in the cell culture media so their concentration in the vicinity of the macrophages

increases, leading to further uptake. Of note, the influence of the sedimentation processes on cell uptake were discussed previously (Cho et al., 2011; Yazdimamaghani et al., 2018).

[Figure 4]

3.4 Study of NP internalization kinetics by confocal microscopy

Whereas NTA enabled to quantify the NPs internalization process by measuring their decreasing concentration in the cell culture media over time, confocal microscopy is a complementary technique, as it allows to directly visualize the NPs' presence inside the macrophages or on their membrane. As an example, a typical image of a J774A.1 macrophage having been in contact with NPs-E for 2 h is presented in **Fig. 5. A** and **B**. A large number of NPs (green spots) can be observed inside the cytoplasm as well as on the cell membrane (red) (the full stack of images can be seen in **Supplementary material 3**). A whole 3D reconstruction of the cell can be conveniently obtained by confocal microscopy (rotating reconstructions are available in **Supplementary material 4** and **5**). However, we intended here to go steps beyond by quantifying the number of internalized NPs in each cell. To do so, the free ImageJ macro Particle_In_Cell-3D was updated and used here (https://imagejdocu.tudor.lu/macro/particle_in_cell-3d) (Torrano et al., 2013).

Briefly, the program analyzes images stacks where both cell membranes and NPs have to be fluorescently marked in order to create an accurate 3D representation of the cell with the objects inside, and to quantify the said objects. In **Fig. 5. C** is displayed the mask that the macro creates before producing the 3D representation with the help of the ImageJ plugin 3D Viewer (**Fig. 5. D**). The virtual cell can then be rotated and cut open in order to observe the internalized NPs (**Fig. 5. E** and **F**). Thus, when a sufficient number of cells is analyzed, Particle_In_Cell-3D could serve as a statistical tool to quantify, for each time point in a kinetic study, the mean number of NPs

346 internalized by immune cells.

347 [Figure 5]

348 In **Fig. 6. A** can be seen a group of macrophages after 2 h of incubation with NPs-E. Surprisingly,
349 some of them internalized large amounts of objects, while others only internalized a few of them.
350 Particle-In-Cell_3D can serve as a means to prove and support this observation. Indeed, six
351 representative cells were analyzed. In this method, the quantification is based on the total
352 fluorescence (i.e. pixel intensity) of the detected NPs. While for some cells, the total fluorescence
353 intensity was about 3×10^6 (arbitrary unit), for other cells, the measured value for intracellular
354 NPs was around 22×10^6 (arbitrary unit). In short, the macro confirmed that the amount of NPs
355 internalized by single cells greatly vary, with neighboring cells having a difference of up to seven
356 times in the quantity of intracellular objects.

357 In **Fig. 6. B**, **C**, **D** and **E** are studied different cells for each time point of the kinetic study. Up to
358 2 h of incubation, internalized NPs appear as sharp and individualized signals. However, the
359 more time passes, the more those signals appear as large and diffuse halos, making it harder to
360 discriminate one from another. Knowing that Rho was covalently bound to the NPs-E, this
361 change probably indicates that NPs degrade inside the macrophages, releasing their Rho label,
362 which produces a diffuse signal around the visualized objects. Possibly, this degradation process
363 is accelerated by the acidic microenvironment inside the lysosomes. In order to study this
364 phenomenon further, it will be necessary to decipher the involved internalization mechanisms.

365 [Figure 6]

366 ## 4. Conclusion

367 Fluorescent PLGA NPs were prepared by nanoprecipitation and emulsification-solvent
368 evaporation methods. The latter method gave larger and more polydisperse populations. NTA

based on tracking individual NPs was more precise than DLS to identify the various populations within a sample.

We have demonstrated the feasibility of an easy-to-use technique for the quantification of polymeric NPs internalization by immune cells, a necessary step in deciphering the interactions between potential drug nanocarriers and the physiological medium. We propose a use of NTA which has never been described before and combine the results to those provided by a freely available ImageJ macro for a precise evaluation of internalization kinetics.

This work presents a proof of concept of the method. In further studies, this technique could be used on larger scales to test several formulations of NPs and identify the most suited ones for the use they are destined to. For example, the impact of size, shape, surface charge and coating on internalization kinetics could easily be tested.

Besides, this method could also help to decipher the internalization cellular mechanisms involved depending on the analyzed NPs, using for example several internalization inhibitors such as chlorpromazine, nystatin or dynasore. Ultimately, the strategy presented here could be used for *in vitro* tests before the *in vivo* evaluation of the NPs formulations.

Acknowledgements

This project has received financial support from the CNRS through the 80 Prime program. We acknowledge support from the French Agence Nationale de la Recherche (ANR) under the grant "SoftGlue" (ANR-20-CE19-0020) and from the Labex NanoSaclay (ANR-10-LABX-0035). We thank the platform CPBM/CLUPS/LUMAT FR2764. The present work has benefited from the Imagerie-Gif core facility, supported by ANR (ANR-11-EQPX-0029 / Morphoscope, ANR-10-INBS-04 / FranceBioImaging; ANR-11-IDEX-0003-02 / Saclay Plant Sciences).

References

Boltnarova, B., Kubackova, J., Skoda, J., Stefela, A., Smekalova, M., Svacinova, P., Pavkova, I., Dittrich, M., Scherman, D., Zbytovska, J., Pavek, P., Holas, O., 2021. PLGA based nanospheres as a potent macrophage-specific drug delivery system. Nanomaterials 11, 749–763. 10.3390/nano11030749

Chaupard, M., de Frutos, M., Gref, R., 2021. Deciphering the structure and chemical composition of drug nanocarriers: from bulk approaches to individual nanoparticle characterization. Part. Part. Syst. Char. 38(9), 2100022. 10.1002/ppsc.202100022

Chicea, D., 2012. A study of nanoparticle aggregation by coherent light scattering. Curr. Nanosci. 8(2), 259–265. 10.2174/157341312800167704

Cho, E. C., Zhang, Q., Xia, Y., 2011. The effect of sedimentation and diffusion on cellular uptake of gold nanoparticles. Nat. Nanotechnol. 6, 685–391. 10.1038/nnano.2011.58

Filipe, V., Hawe, A., Jiskoot, W., 2010. Critical evaluation of nanoparticle tracking analysis (NTA) by NanoSight for the measurement of nanoparticles and protein aggregates. Pharm. Res. 27, 796–810. 10.1007/s11095-010-0073-2

Finean, J. B., Rumsby, M. G., 1963. Negatively stained lipoprotein membranes. Nature 200,

1340. 10.1038/2001340b0

Gref, R., Minamitake, Y., Peracchia, M. T., Trubetskoy, V., Torchilin, V., Langer, R., 1994. Science 263, 1600–1603. 10.1126/science.8128245

Gref, R., Couvreur, P., Barratt, G., Mysiakine, E., 2003. Surface-engineered nanoparticles for multiple ligand coupling. Biomaterials 24, 4529–4537. 10.1016/s0142-9612(03)00348-x

Hernández-Giottonini, K. Y., Rodríguez-Córdova, R. J., Gutiérrez-Valenzuela, C. A., Peñuñuri-Miranda, O., Zavala-Rivera, P., Guerrero-Germán, P., Lucero-Acuña, 2020. PLGA nanoparticle preparations by emulsification and nanoprecipitation techniques: effects of formulation parameters. Roy. Soc. Ch. 10, 4218–4231. 10.1039/c9ra10857b

Hoo, C. M., Starostin, N., West, P., Mecartney, M. L., 2008. A comparison of atomic force microscopy (AFM) and dynamic light scattering (DLS) methods to characterize nanoparticle size distributions. J. Nanopart. Res. 10, 89–96. 10.1007/s11095-010-0073-2

Hoshyar, N., Gray, S., Han, H., Bao, G., 2016. The effect of nanoparticle size on *in vivo* pharmacokinetics and cellular interaction. Nanomedicine 11, 673–692. 10.2217/nnm.16.5

Jones, A-A. D. III, Mi, G., Webster, T. J., 2019. A status report on FDA approval of medical devices containing nanostructured devices. Trends Biotechnol. 37, 117–120. 10.1016/j.tibtech.2018.06.003

Legrand, P., Lesieur, S., Bochot, A., Gref, R., Raatjes, W., Barratt, G., Vauthier, C., 2007. Influence of polymer behaviour in organic solution on the production of polylactide nanoparticles by nanoprecipitation. Int. J. Pharm. 344, 33–43. 10.1016/j.ijpharm.2007.05.054

Miladi, K., Sfar, S., Fessi, H., Elaissari, A., 2016, in: Vauthier, C., Ponchel, G. (Eds.), Polymer nanoparticles for nanomedicines. Springer, Cham, 17–53. 10.1007/978-3-319-41421-8_2

Nguyen, T., Francis, M. B., 2003. Practical synthetic route to functionalized rhodamine dyes.

Org. Lett. 5, 3245–3248. 10.1021/ol035135z

Nicolete, R., dos Santos, D. F., Faccioli, L. H., 2011. The uptake of PLGA micro or nanoparticles by macrophages provokes distinct *in vitro* inflammatory response. Int. Immunopharmacol. 11, 1557–1563. 10.1016/j.intimp.2011.05.014

Pancani, E., Mathurin, J., Bilent, S., Bernet-Camard, M.-F., Dazzi, A., Deniset-Besseau, A., Gref, R., 2018. High-resolution label-free detection of biocompatible polymeric nanoparticles in cells. Part. Part. Syst. Char. 35, 1700457. 10.1002/ppsc.201700457

Rattan, R., Bhattacharjee, S., Zong, H., Swain, C., Siddiqui, M. A., Visovatti, S. H., Kanthi, Y., Desai, S., Pinsky, D. J., Goonewardena, S. N., 2017. Nanoparticle-macrophage interactions: a balance between clearance and cell-specific targeting. Bioorgan. Med. Chem. 25, 4487–4496. 10.1016/j.bmc.2017.06.040

Sharma, A., Kontodimas, K., Bosmann, M., 2021. Nanomedicine: a diagnostic and therapeutic approach to COVID-19. Front. Med. 8, 648005. 10.3389/fmed.2021.648005

Soo, C. Y., Song, Y., Zheng, Y., Campbell, E. C., Riches, A. C., Gunn-Moore, F., Powis, S. J., 2012. Nanoparticle tracking analysis monitors microvesicle and exosome secretion from immune cells. Immunology 136, 192–197. 10.1111/j.1365-2567.2012.03569.x

Torrano, A. A., Blechinger, J., Osseforth, C., Argyo, C., Reller, A., Bein, T., Michaelis, J., Bräuchle, C., 2013. A fast analysis method to quantify nanoparticle uptake on a single cell level. Nanomedicine 8, 1815–1828. 10.2217/nnm.12.178

Ulbrich, K., Holá, K., Šubr, V., Bakandritsos, A., Tuček, J., Zbořil, R., 2016. Chem. Rev. 116, 5338–5431. 10.1021/acs.chemrev.5b00589

Varenne, F., Makky, A., Gaucher-Delmas, M., Violleau, F., Vauthier, C., 2016. Multimodal dispersion of nanoparticles: a comprehensive evaluation of size distribution with 9 size measurement methods. Pharm. Res. 33, 1220–1234. 10.1007/s11095-016-1867-7

Wu, S., Helal-Neto, E., dos Santos Matos, A. P., Jafari, A., Kozempel, J., de Albuquerque Silva, Y. J., Serrano-Larrea, C., Junior, S. A., Ricci-Junior, E., Alexis, F., Santos-Oliveira, R., 2020. Radioactive polymeric nanoparticles for biomedical application. Drug Deliv. 27, 1544–1561. 10.1080/10717544.2020.1837296

Yazdimamaghani, M., Barber, Z. B., Moghaddam, S. P. H., Ghandehari, H., 2018. Influence of silica nanoparticle density and flow conditions on sedimentation, cell uptake, and cytotoxicity. Mol. Pharm. 15, 2372–2383. 10.1021/acs.molpharmaceut.8b00213

Zhao, Z., Ukidve, A., Krishnan, V., Mitragotri, S., 2019. Effect of physicochemical and surface properties on *in vivo* fate of drug nanocarriers. Adv. Drug Deliver. Rev. 143, 3–21. 10.1016/j.addr.2019.01.002

Zheng, Y., Campbell, E. C., Lucocq, J., Riches, A., Powis, S. J., 2012. Monitoring the Rab27 associated exosome pathway using nanoparticle tracking analysis. Exp. Cell Res. 319, 1706–1713. 10.1016/j.yexcr.2012.10.006

Zielińska, A., Carreiró, F., Oliveira, A. M., Neves, A., Pires. B, Venkatesh, D. N., Durazzo, A., Lucarini, M., Eder, P., Silva, A. M., Santini, A., Souto, E. B., 2020. Polymeric nanoparticles: production, characterization, toxicology and ecotoxicology. Molecules 25, 3731–3750. 10.3390/molecules25163731

Captions to Figures

Fig. 1. A. Schematic representation of the DLS method. A laser beam is aimed at the sample. When crossing the laser beam, NPs scatter the light, the larger ones more than the smaller ones. The information is treated in order to estimate the mean hydrodynamic diameter of NPs in the sample. **B.** Schematic representation of the NTA method. Dynamic light scattering is also involved as NPs are illuminated by a laser beam. With an optical microscope coupled to a

camera, the NPs' trajectories are recorded and analyzed (as depicted on the right), which serves to determine their individual hydrodynamic diameters accurately.

Fig. 2. A and B. TEM images of NPs-P and NPs-E respectively. **C and D.** NTA profiles of NPs-P and NPs-E in Milli-Q water respectively, with (solid line) or without (dotted line) a fluorescence filter. **E and F.** NTA profiles of NPs-P and NPs-E in cell culture medium respectively.

Fig. 3. A and B. Screenshots taken during the NTA analysis of NPs-P and NPs-E in Milli-Q water respectively. The recorded video is played in the background while the NPs' trajectories (red lines) are analyzed and the size distribution graph is calculated at the same time (blue curve). During the analysis, the graph changes every second, cumulating the information provided by the recorded video. **C and D.** Size distribution graphs comparing the results obtained with NTA and DLS (number distribution) for NPs-P and NPs-E in Milli-Q water respectively.

Fig. 4. Internalization curve of NPs-E inside J774A.1 macrophages (red curve) and control corresponding to NPs-E incubated under the same conditions, but without J774A.1 macrophages (gray curve).

Fig. 5. A and B. J774A.1 macrophage with internalized NPs-E (2 h of incubation) observed by white light and fluorescence confocal microscopy (cell membrane in red, NPs in green) respectively. **C.** Cell mask created by the macro Particle_In_Cell-3D (https://imagejdocu.tudor.lu/macro/particle_in_cell-3d). **D, E and F.** 3D representation of the macrophage created by the macro, under different angles.

Fig. 6. A. Group of J774A.1 macrophages with internalized NPs-E (2 h of incubation) observed by fluorescence confocal microscopy (cell membranes in red, NPs in green). **B, C, D and E.**

J774A.1 macrophages with internalized NPs at different times of incubation (1 h, 2 h, 4 h and 24 h respectively).

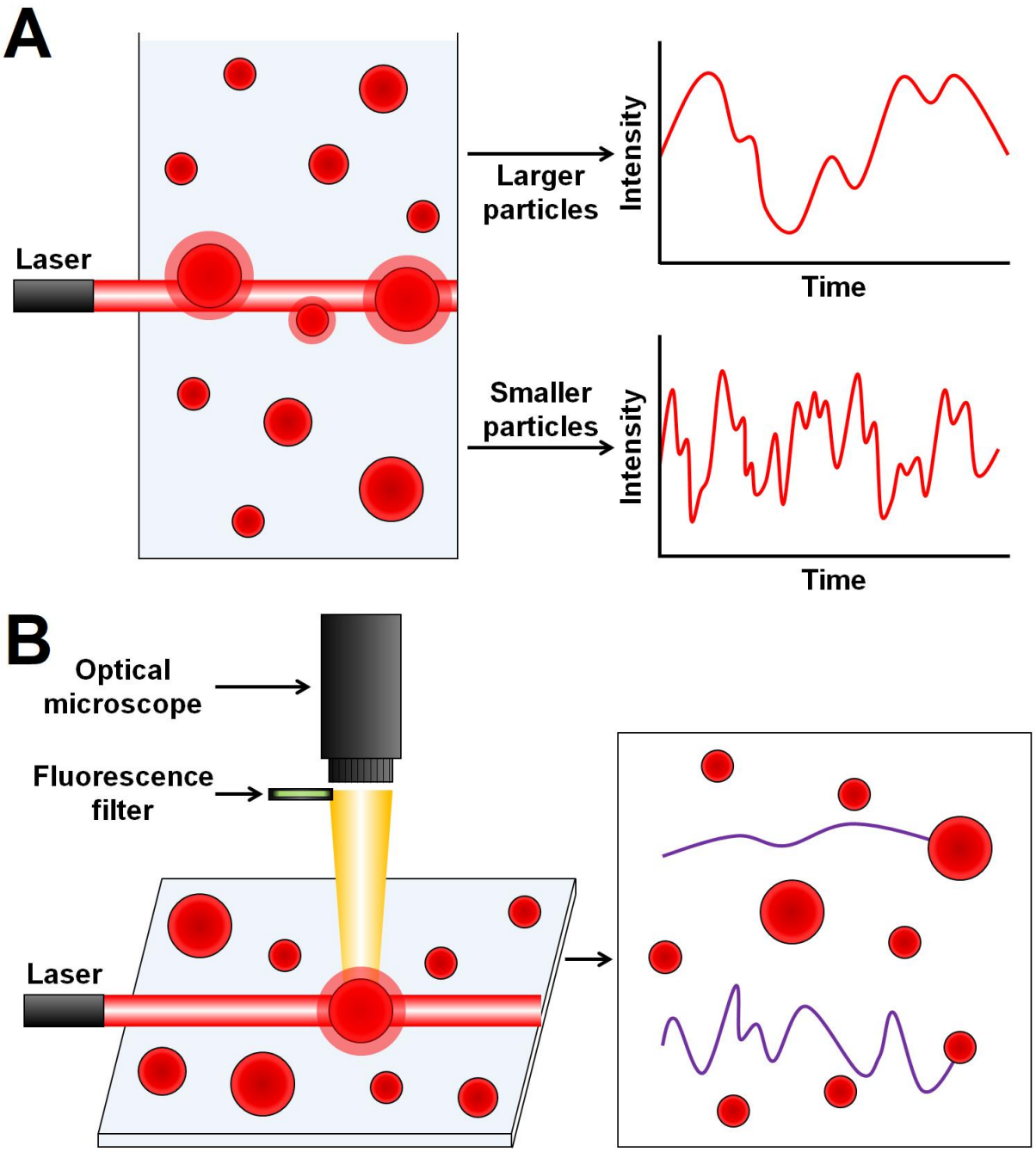
A
Laser
Larger particles
Intensity
Time
Smaller particles
Intensity
Time
B
Optical microscope
Fluorescence filter
Laser

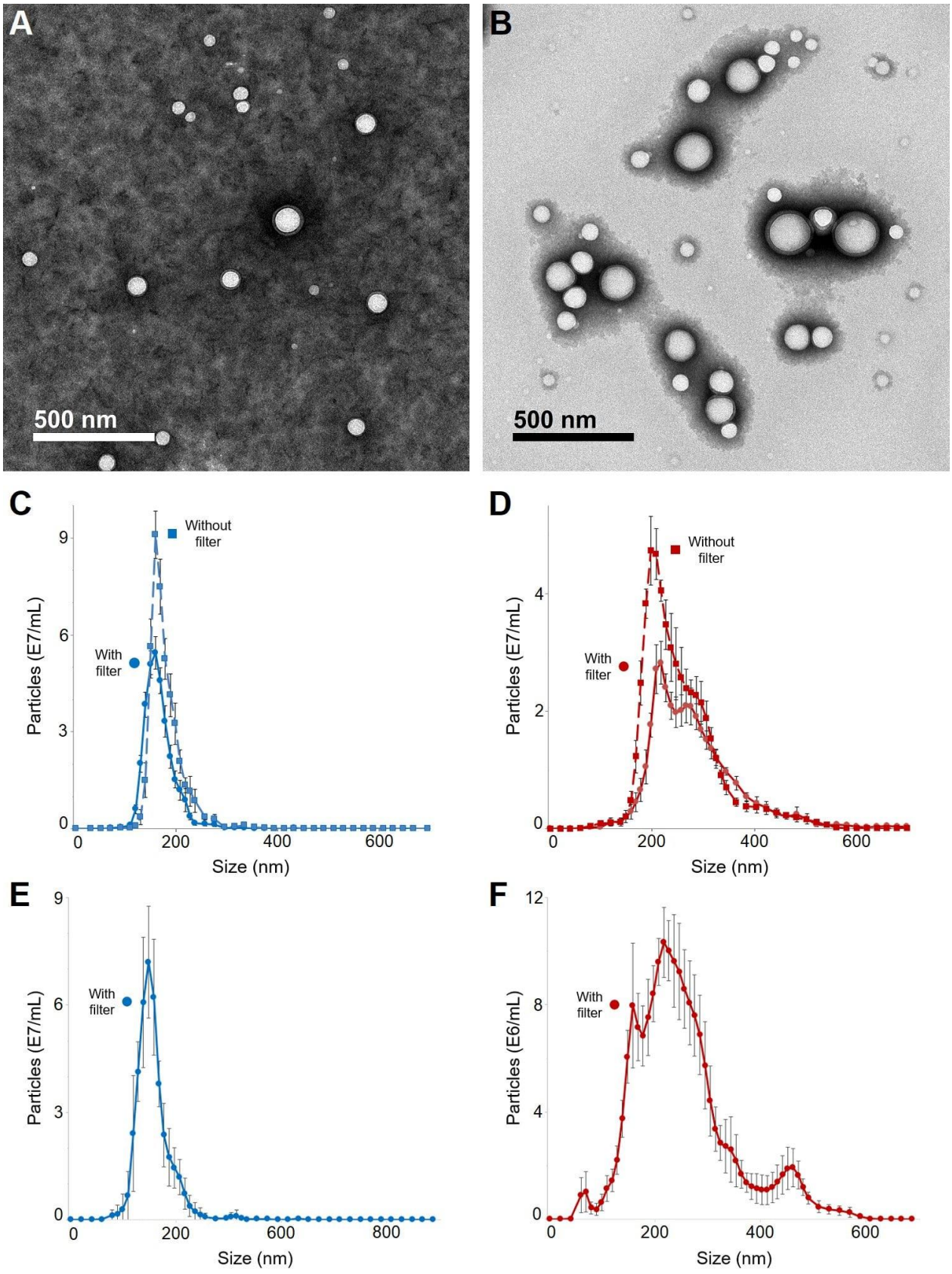
A
500 nm
B
500 nm
C
Without filter
With filter
Particles (E7/mL)
Size (nm)
D
Without filter
With filter
Particles (E7/mL)
Size (nm)
E
With filter
Particles (E7/mL)
Size (nm)
F
With filter
Particles (E6/mL)
Size (nm)

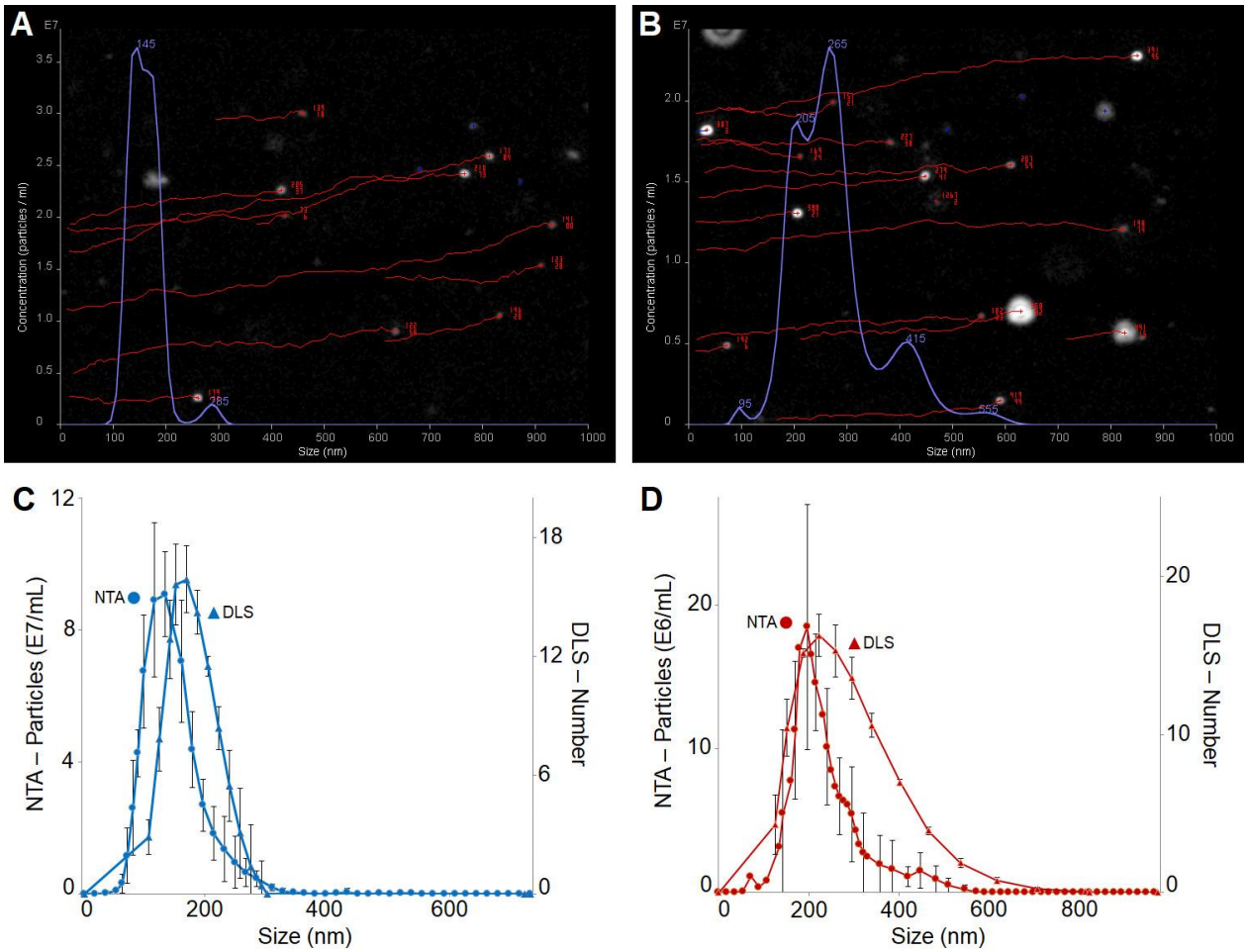
A
E7
Concentration (particles / ml)
Size (nm)
145
285
B
E7
Concentration (particles / ml)
Size (nm)
265
205
415
95
555
C
NTA – Particles (E7/mL)
DLS – Number
NTA
DLS
Size (nm)
D
NTA – Particles (E6/mL)
DLS – Number
NTA
DLS
Size (nm)

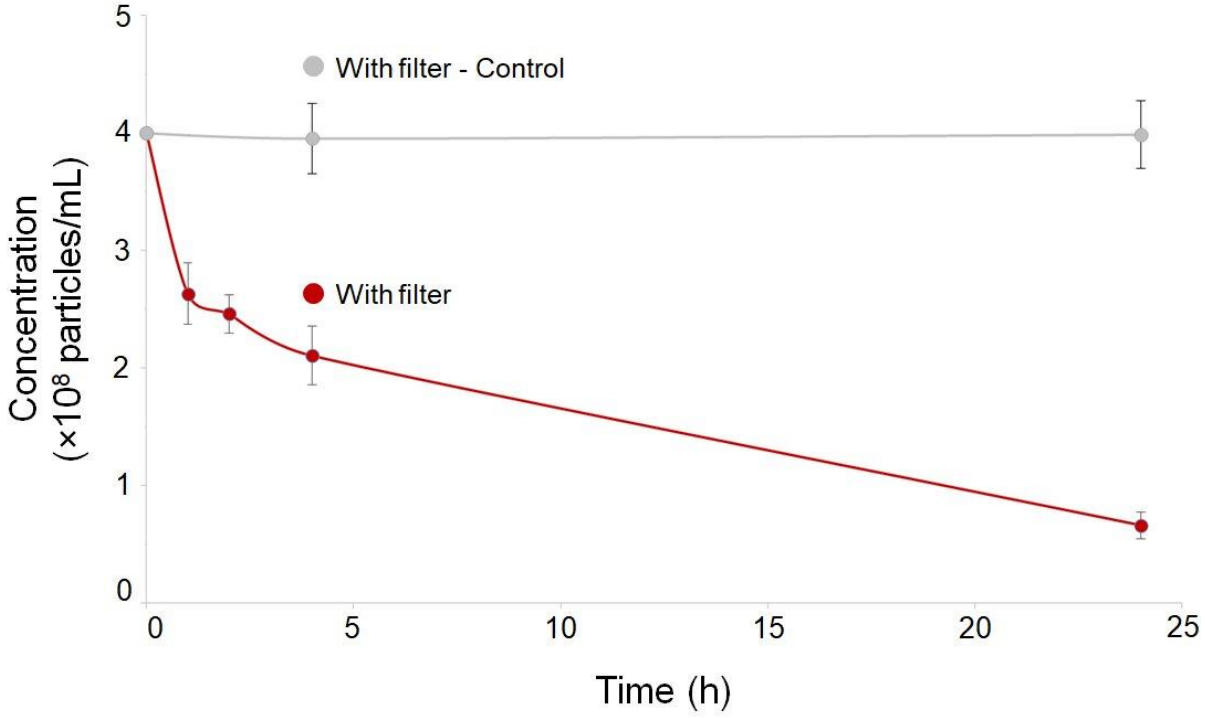
With filter - Control
With filter
Concentration
(×10⁸ particles/mL)
Time (h)
0
1
2
3
4
5
0
5
10
15
20
25

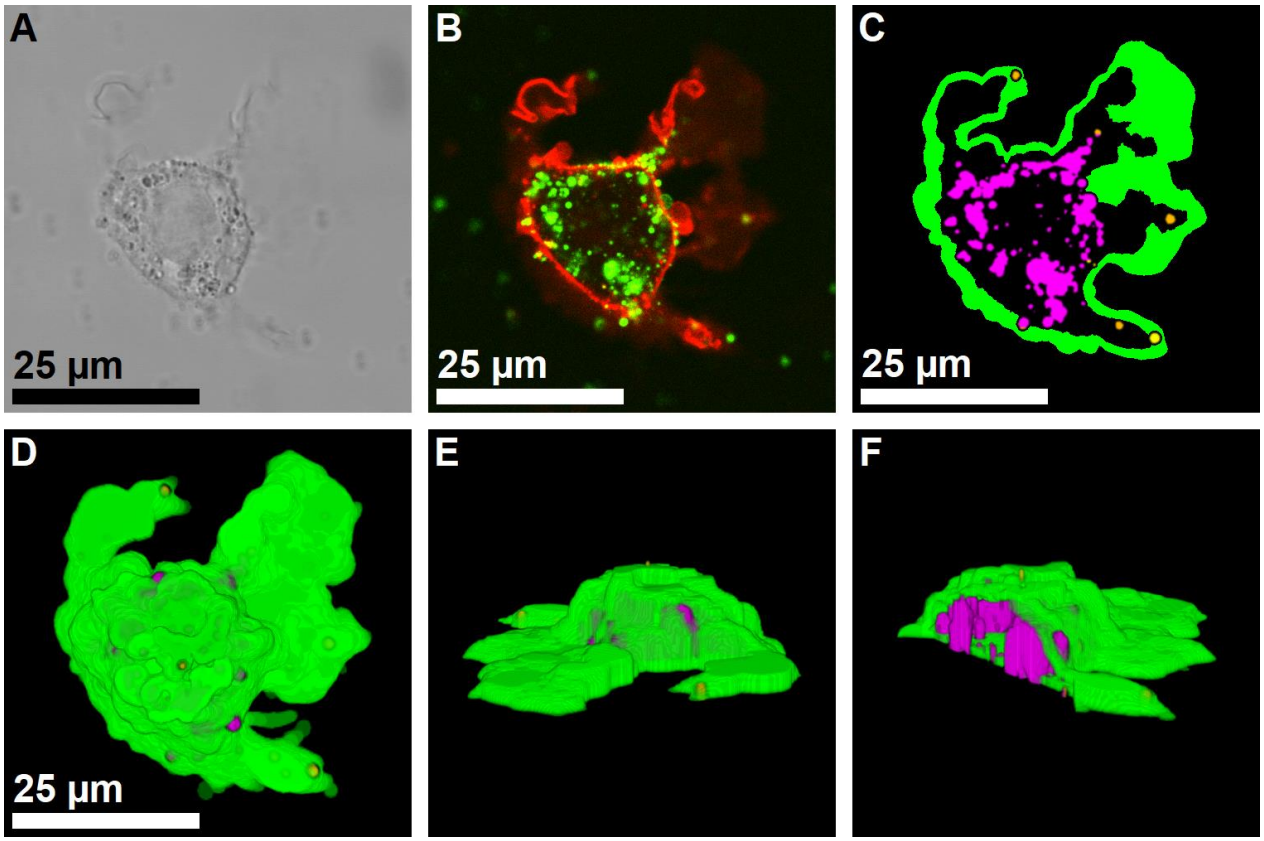
A
25 µm
B
25 µm
C
25 µm
D
25 µm
E
F

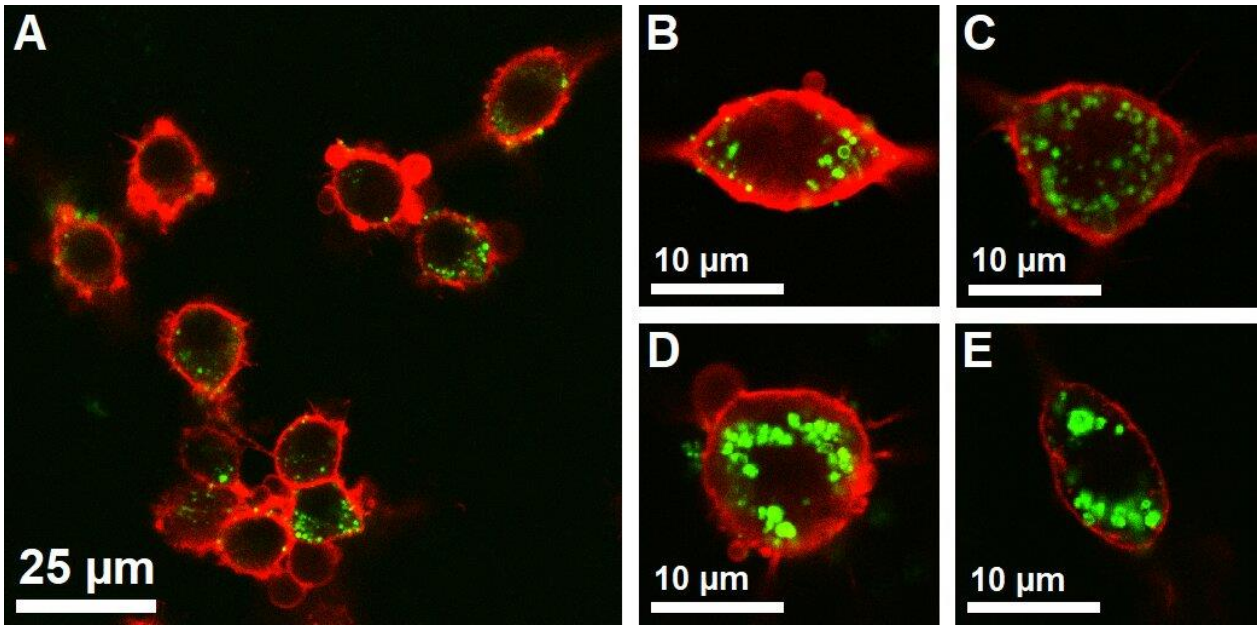
A
25 µm
B
10 µm
C
10 µm
D
10 µm
E
10 µm

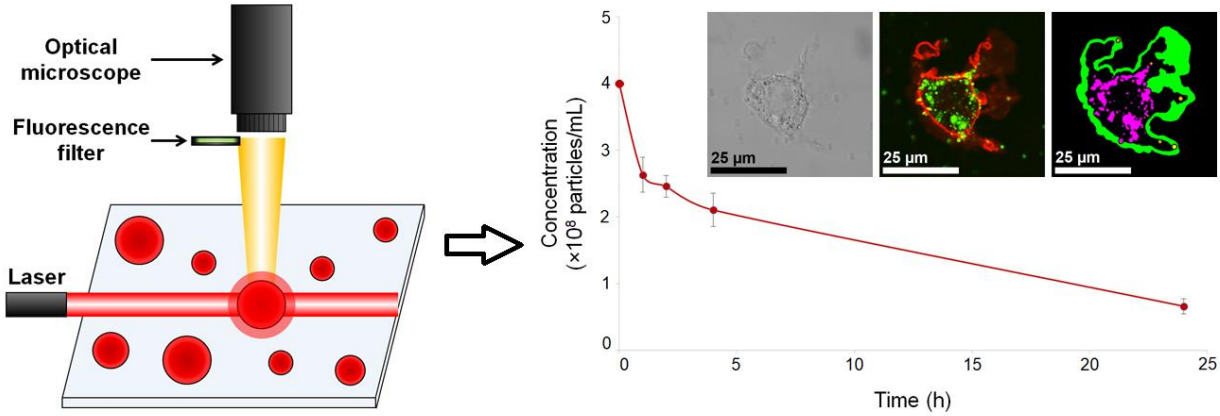

Nanoparticle tracking analysis allows a direct measurement of the amount of nanoparticles which did not interact with immune cells. Complementary techniques (such as confocal microscopy) allow to visualize nanoparticles which did interact with such cells.